CAAP Quarterly Report

[01/02/2025]

Project Name: "All-in-One Multifunctional Cured-In-Place Structural Liner for Rehabilitating of Aging Cast Iron Pipelines"

Contract Number: 693JK32250009CAAP

Prime University: North Dakota State University

Prepared By: [Ying Huang, ying.huang@ndsu.edu, 701-231-7651]

Reporting Period: [09/28/2024 – 12/27/2024]

Project Activities for Reporting Period:

In the 8th quarterly report, Tasks 2.1, 2.2, 3.1, 3.2, 3.3, 3.4, 4.1, 4.2, and 5.1 were carried out as proposed. In this quarter (Quarter 9), the research team has continued to make consistent progress on selected tasks. Summaries of the key activities completed during the 9th reporting period are provided below.

Mid-term Summary: In this quarter, the university research team held a mid-term summary meeting with PHMSA program managers on November 25th, 2024, providing project progress updates to ensure that the tasks align with PHMSA's expectations and guidelines.

Task 2.1 Preparation of Vitrimer Epoxy Resins, Characterization, and Optimization of the Processing and Curing Conditions (90%): In the last quarter, the newly proposed self-healing resin (DFA:RDA) demonstrated significantly lower glass transition temperatures (T_gs),. The research team (Dr. Long Jiang and Austin Knight, Ph. D. student from NDSU) incorporated catalysts into the self-healing polymers at various concentrations to determine the optimal formulation. The key findings are summarized below:

(1) Transesterification Catalyst in Newly Developed DFA:RDA Resin: The transesterification catalyst used in this report is a hydrated salt, which can be dehydrated by heating to remove the bonded water from the powder. The powder was dried and resulting in a higher weight loss than the theoretical weight of water expected to be lost. However, after UV-curing and dilatometry tests, it was evident that the dehydrated powder inhibited UV-curing, even at low concentrations (5 mol%), likely due to the potential decomposition of the catalyst into UV-absorbing or reflecting molecules (Figure 1(a)). Extended curing times did not improve the degree of cure (Figure 1(b)). Subsequent tests using the catalyst without drying showed more complete resin curing, leading to the decision to use the undried catalyst in all further experiments (Figure 1(c)). These tests also revealed a decrease in transition temperatures but showed a general absence of prominent vitrimer behavior in the dilatometry curves.

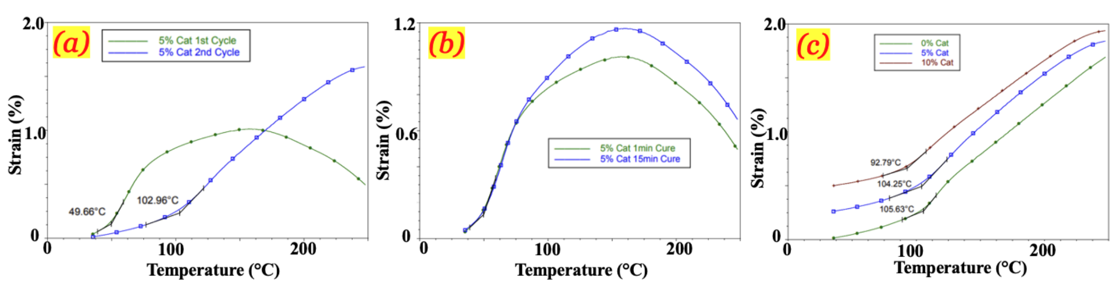

Figure 1. The dilatometry results for DFA:RDA formulations with dried 5% catalyst: (a) the first and second heating cycle, (b) UV-curing after 1 and 15mins, and (c) increased catalyst amount.

Task 3.1 High Mechanical Performance (90%) and **Task 3.2** Enhanced bonding performance (70%): During this reporting period, the research team (Dr. Ying Huang, Dr. Xingyu Wang, and Muhammad Imran Khan, Master student from NDSU) continued experimental study on nanoparticle reinforcement on the developed self-healing polymer (DFMA:RDMA). The key findings are provided below:

(1) Flexural Creep Test of Self-Healing Polymer with Nanoparticles (NPs): Based on the flexural creep results, a logarithmic regression was applied to the data from the first 100 hours of testing to predict the strain for each specimen at 1000 hours. Using these predicted strains at 1000 hours, the flexural stress required to achieve strains of 1%, 1.5%, and 2% was calculated for each formulation (Figure 2(d)). The isochronous stress-strain curves presented in the standard exhibit a clear logarithmic trend (Figure 2(a)–(c)). The ND formulation showed the lowest flexural modulus, which may be attributed to the addition of ND, making the polymer matrix more ductile compared to the neat polymer (consistent with previous tensile test results). This increased ductility could be advantageous when liners are subjected to impact, as ductile materials are better able to maintain their structural integrity under such conditions.

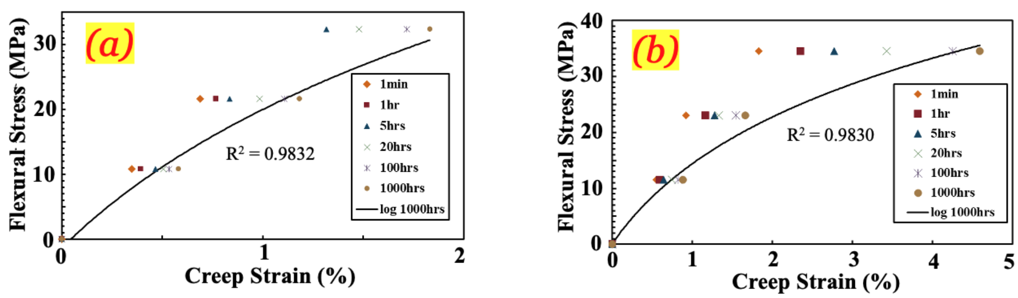

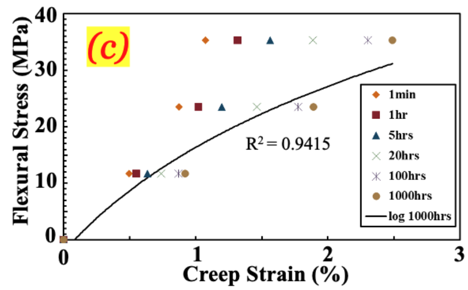

(d)

Specimen	Stress (MPa) required for a specific strain after 1000 hours			Flexural Modulus (GPa)
	1.0%	1.5%	2.0%	
Neat	20.0	26.9	32.5	199
0.5% ND	14.4	19.0	22.7	160
0.5% NS	16.4	22.3	27.2	180

Figure 2. Results of the flexural creep test for (a) neat, (b) 0.5% ND, and (c) 0.5% NS.

(2) Bonding Test of Self-Healing Polymer with Nanoparticles: The single lap shear (SLS) test for the neat, 0.5% ND, and 0.5% NS samples revealed that the neat specimens did not show yielding, the 0.5% ND and 0.5% NS samples exhibited yielding behavior. Although the 0.5% ND and NS samples yielded at a lower stress than the failure point of the neat samples, this yielding resulted in higher ultimate strength, ultimate strain, and toughness for these formulations (Figure 3).

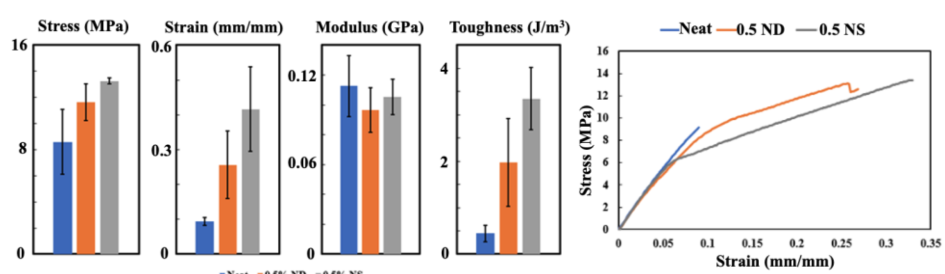

Figure 3. Bonding properties of self-healing polymers with NPs.

Task 3.3. Reducing the Permeability and Investigating the Interfacial Bonding Chemical Analysis (75%): Previously, the research team (Dr. Liangliang Huang, Qiuhao Chang, Ph. D. student from University of Oklahoma) successfully applied the REACTOR method in reactive molecular dynamics simulations of polymer systems to model vitrimer reactions, to work with the developed self-healing polymer resins. Furthermore, we explored the influence of various parameters on the simulations using the REACTOR method, focusing on optimizing the modeling process and understanding the reaction dynamics:

(1) Effects of Initial Atom: As shown in Figure 4(a), reactive molecular dynamics simulations were used to model the transesterification reaction between bisphenol A-glycidyl methacrylate (Bis-GMA) and 2-Hydroxyethyl Methacrylate (2-HEMA). For a reactive model, both a map file and template files representing the system before and after the reaction are required. The map file specifies the initial and terminal atoms involved in the reaction. In our model, various tests were conducted to identify the most suitable starting atoms for the reaction. Initially, the oxygen atom in Bis-GMA and the hydrogen atom from the hydroxyl group in 2-HEMA were selected as the initial atoms. However, it was observed that the hydrogen atom in 2-HEMA was frequently attracted to other oxygen atoms within 2-HEMA due to electrostatic forces, preventing effective interaction with the initial atom in Bis-GMA. A more effective strategy involved selecting the carbon atom in Bis-GMA and the oxygen atom in 2-HEMA as the initial atoms (Figure 4(b)), which resolved the interference issue and facilitated smoother reaction modeling.

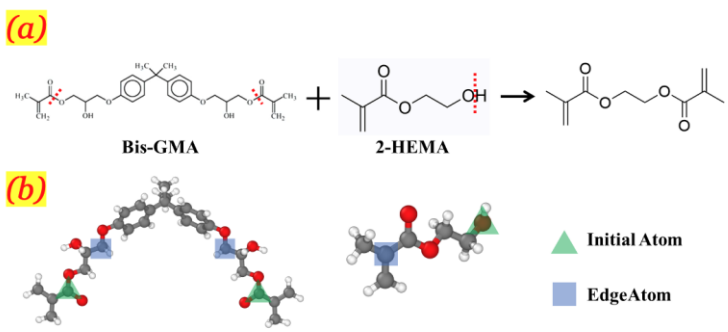

Figure 4. (a) Transesterification between Bis-GMA and 2-HEMA; (b)Reactive sites of Bis-GMA and 2-HEMA monomers for a reactive vitimite model.

(2) Effects of Temperature: After defining the map file and template files required for the reaction simulation, we constructed a system consisting of 10 pairs of Bis-GMA and 2-HEMA molecules. The reaction was successfully simulated under conditions of 300 K, 1 atm pressure, and a test density of 0.1 g/cm³. To further explore the effect of temperature on the reaction dynamics, we conducted additional tests by varying the temperature while keeping other parameters constant. Simulations were carried out at 300 K, 600 K, and 900 K. The results revealed that at elevated temperatures of 600 K and 900 K, the simulation system encountered errors related to missing bonds or atoms. We believe that these errors are due to the increased kinetic energy at higher temperatures, which causes atoms to move more rapidly and, in some cases, drift too far apart during the reaction process. This excessive separation between atoms likely disrupts the bond formation necessary for the reaction, leading to inaccuracies in the simulation.

(3) Effects of Density: To examine the effect of density on the reaction process, we utilized the NPT ensemble to simulate systems at densities of 1.0 g/cm³ and 0.1 g/cm³, under conditions of 300 K and 1 atm, as shown in Figure 5. At the lower density of 0.1 g/cm³, approximately a simulation time of 0.76 ns could result in the expected successful reactions of the 10 pairs. In contrast, at the higher density of 1.0 g/cm³, only two pairs underwent reaction within 1 ns. This variation in reaction rate can be explained by the increased molecular mobility at lower densities, where molecules have greater freedom to move and interact, leading to better reaction

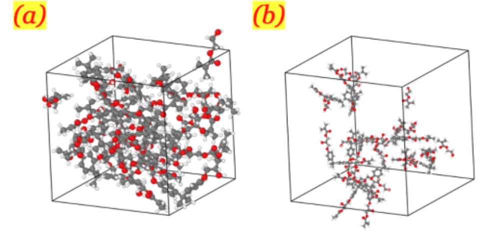

Figure 5. Models with different densities: (a) 1.0 g/cm^3; (b) 0.1 g/cm^3.

kinetics. Conversely, at higher densities, molecular motion becomes more restricted due to the limited available space, which hinders the ability of molecules to reach the required proximity for reactions to occur. This restriction reduces the likelihood of successful collisions between reactive sites, significantly slowing down the reaction process. These findings emphasize the critical role that molecular density plays in controlling the dynamics of reactions in polymer systems, where lower densities promote faster reaction rates, and higher densities lead to a slower, more constrained reaction environment.

(4) Effects of PPPM: In addition, during the simulation testing process, it was observed that setting the precision parameters for the PPPM (Particle-Particle Particle-Mesh) method too low could lead to the error of bond atoms missing. In the examples provided by the REACTOR method, the default PPPM precision value is typically set at 1e-4, whereas in most cases, a value of 1e-5 is commonly used. The smaller the PPPM parameter, the higher the computational accuracy for simulating long-range electrostatic interactions. Reducing the precision value from 1e-4 to 1e-5 leads to more accurate calculations of long-range forces, which can help minimize errors in the simulation of charge interactions. However, while this increase in accuracy is good for capturing long-range interactions, it can pose challenges for reaction simulations. Specifically, when the precision parameter is set too low, atomic exchange between molecules can occur if the distance between starting atoms falls below a predefined reaction threshold.

Task 3.4 Finite Element Numerical Analysis to Guide the Design of the Developed High-performance Healable CIPP Structural Liner (85%): During this reporting period, the research team (Dr. Chengcheng Tao, Junyi Duan, Ph.D. student from Purdue University) started finite element analysis (FEA) on pipelines with CIPP liners to investigate the response of the pipe-liner system under impact action; the study closely collaborated with experimental results in Task 4.1. Additionally, the fracture behavior of the liner system was also simulated and worked with compact tension tests. The findings are summarized below:

(1) Finite Element Analysis of Dynamic Impact on Liner-protected Substrates: To investigate the dynamic impact and damage in liner-protected substrates, we use the finite element software ABAQUS to perform a dynamic explicit analysis. Figure 6(a) shows the FEA model used in this study. The bottom edges of the substrate are clamped to restrict movement in all directions. To capture the transient response at the impact area, additional partitions are created in the middle of the substrate, and a finer mesh is used. Figure 6(b) presents the displacement distribution at the first impact. Displacement and reaction forces are plotted in Figure 6(c), showing impacts at 0.143 s, 0.327 s, and 0.444 s, with gradually decreasing displacement and reaction forces. The peak displacement and reaction force are 2.47 mm and 18.5 N, respectively. Additionally, a residual displacement of 0.046 mm is observed at the center of the plate at the final stage.

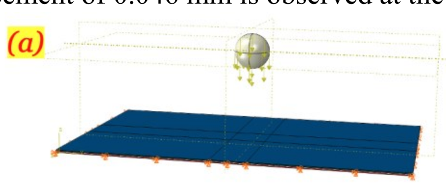

Figure 6. (a) FEA model of dynamic impact on liner-protected substrate. And FEA results of dynamic impact: (b) vertical displacement at the first impact; (c) vertical displacement ad reaction force versus time.

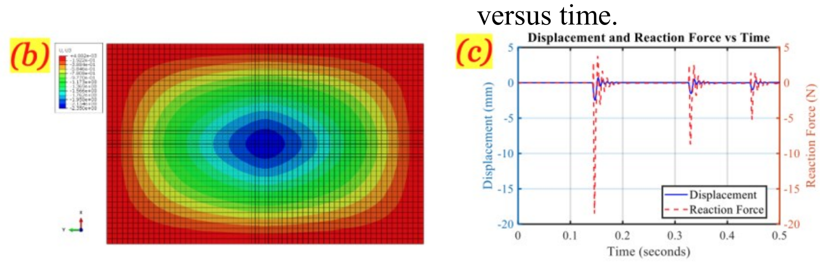

(2) Finite Element Analysis on Fracture Behavior of Liner-protected Substrates: Fracture toughness represents a material's ability to resist crack propagation, which is particularly critical for brittle materials like CIPP liners, where failure often occurs due to crack growth. In this task, a compact tension finite element model was developed using the geometric details from the compact tension test to investigate fracture toughness, as shown in Figure 7. The extended finite element method (XFEM) was employed in ABAQUS to simulate crack propagation. An initial crack was introduced at the crack tip to initiate the crack development process. In the model setup, uniform displacement control was applied at the top hole, while the bottom hole was constrained to allow only out-of-plane rotation. Figure 7 also compares the experimental results with the FEA simulation, revealing fluctuating vertical cracks in both cases. The results align well with the fiber fabric orientation (zero degrees) within the liner, confirming the validity of the model.

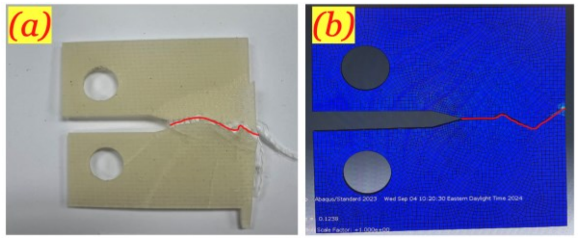

Figure 7. The crack patterns after failure. (a) Experiment result; (b) FEA simulation result.

Task 4.1 Development of Embedded Distributed Fiber Optic Sensors for Self-sensing Structural Liner (85%), and **Task 4.2** Investigating the Load Transfer between Layers of the CIPP Liner and the Cast-iron Substrate (70%): During this reporting period, the research team (Dr. Ying Huang and Dr. Xingyu Wang) designed and initiated experimental investigations of the smart-liner system under impact loading. The primary objective is to identify the impact location, strain field, and deformation in the smart-liner system. The key findings are summarized below:

(1) Experimental Set-up of the Smart Liner under Impact Loading: As shown in Figure 8, the specimen consists of a 19 × 11-inch steel plate protected by the smart liner (Figure 8(a)), which contains sensors capable of detecting strain distribution across the liner. Additionally, a stainless-steel ball was used to simulate impact by dropping it onto the steel plate The dynamic load is applied by a solid C440 stainless steel ball, dropped freely from a height of 127 mm. For this study, four representative locations were selected for impact testing (Figure 8(b)): the center, two edges, and one corner of the specimen. These locations were chosen because they have varying sensor coverage, resulting in different amounts of strain data being collected. This variation poses unique challenges in identifying the impact location, load, and deformation.

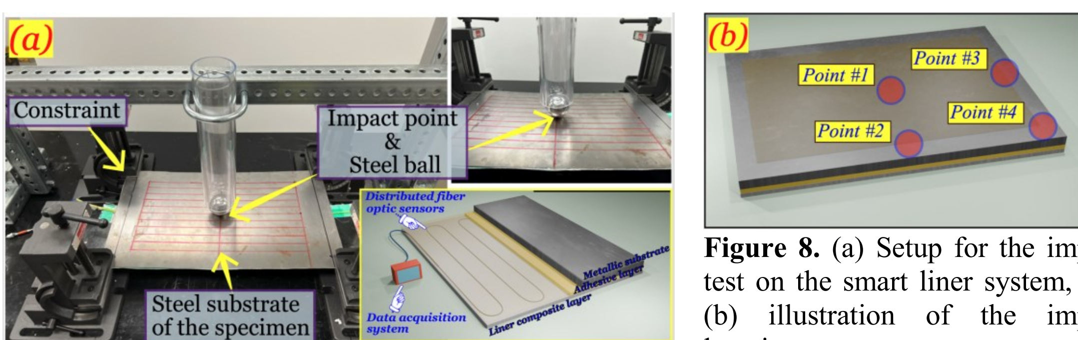

Figure 8. (a) Setup for the impact test on the smart liner system, and (b) illustration of the impact locations.

(2) Identification of Impact Location and Creation of Strain Field: After the specimen was impacted at the four locations (Points 1–4), strain signals were collected and plotted as strain fields based on the geometry of the specimen. The impact locations were easily identifiable, as shown in Figures

9(a) to (d). The largest strain values and distinct strain patterns greatly aided in identifying the impact points. Although the impacts on the edges and corners were less prominent compared to the center of the specimen, the impact locations were still clearly distinguishable. In addition to the 2D strain fields shown in Figures 9(a) to (d), Figure 9(e) presents a 3D visualization of the strain field.

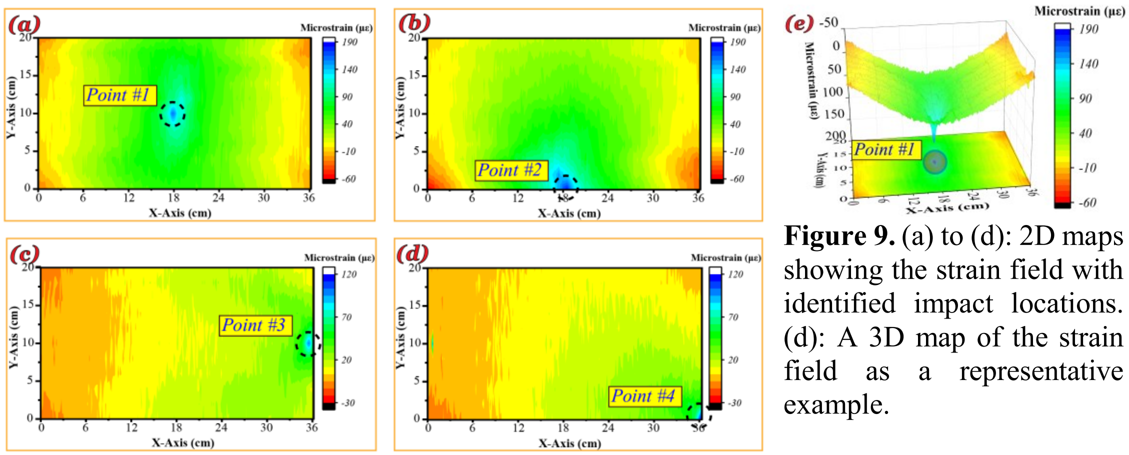

Figure 9. (a) to (d): 2D maps showing the strain field with identified impact locations. (d): A 3D map of the strain field as a representative example.

Task 5.1 Development of CIPP Liner Risk Index for the Pipeline Integrity Management Enhanced by AI Algorithms (65%): During this period, the research team (Dr. Chengcheng Tao, Huaixiao Yan, Ph.D. student from Purdue University) have conducted the risk assessment using a dataset generated from fiber optic sensor (Task 4) for pipeline integrity management, with the results outlined below:

(1) Digital Twin Establishment from Sensor Data: The main purpose of this part is to build a digital-twin model of liner based on the strain distribution data collected from fiber optic sensors. The experimental setting is shown in Figure 10. The pipe has an inner diameter of 12 inches, and the mart liner is applied on the inner wall of the pipe, then the sensors in the smart liner recorded the strain changes. The digital-twin model presented in this study was used for the final moment data. After obtaining the data from distributed sensors, we used linear interpolation to generate the strain field of the other parts. We interpolated four points at a time to obtain the strain inside the rectangle (the red rectangle) formed by these four points. In this way, the approximate strain distribution of a plane can be obtained. The next step is mapping the strain on the plane into real shape to generate the digital twin model. The most accurate method is to read the color on every pixel and map it by transferring its 2-D natural coordinate system into 3-D polar coordinate system. The generated digital twin model has the same shape as our target structure and can provide the strain of every node on the surface.

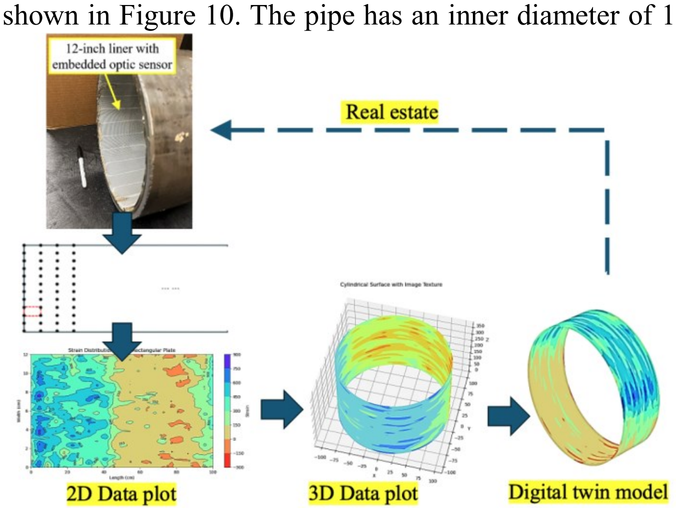

Figure 10. Flowchart for creation of the digital twin model for a pipeline with smart liner system.

Project Financial Activities Incurred during the Reporting Period:

The cost breakdown during the reporting period according to the budget proposal is shown in Table 1.

Table 1. Cost breakdown

Category	Amount spent during Q9
Personnel	
Faculty	$0
Postdoc	$1,249.93
Students (RA and UR)	$13,500.00
Benefits	$677.55
Operating Expenses	
Travel	$0
Materials and Supplies	$846.70
Recharge Center Fee	$7,716.90
Consultant Fee	$1,275.00
Subcontracts	$33,506.53
Indirect Costs	$12,696.04

Project Activities with Cost Share Partners:

The Match fund from NDSU for this project is coming from the tuition of the associated graduate students during their work on this project. During the reporting period (Q9), Zahoor Hussain (100%), Muhammad Imran Khan (100%), Austin Knight (100%), and Tofatun Jannet (46.15%) were working on the project. The tuition for the four students during Q9 was estimated to be $12,520 at a rate of $463.73 per credit.

Project Activities with External Partners:

During this reporting period, George Ragula, our industry consultant, attended all the bi-weekly meetings with the research team.

Potential Project Risks:

No potential risks were noticed during this reporting period.

Future Project Work:

The research team will continue working on Tasks 2.1, 2.2, 3.1, 3.2, 3.3, 3.4, 4.1, 4.2 and 5.1.

Potential Impacts on Pipeline Safety:

Although the previously developed self-healing epoxy (DFMA:RDMA) reinforced with nanodiamonds (ND) demonstrated excellent properties to meet the requirements of the proposal, the research team is further advancing the development of self-healing polymers. The newly proposed self-healing resin (DFA:RDA) shows great potential, requiring lower temperatures for self-healing. Concurrently, significant progress has been made in molecular dynamics simulations to create models for the self-healing polymer developed in this study, providing valuable insights into the mechanisms of self-healing. Meanwhile, finite Element Analysis (FEA), working closely with experimental studies, is focused on investigating the behavior of the smart-liner system under impact loading, a critical factor for pipeline systems. The smart-liner system has proven to be highly effective in identifying impact locations and generating strain fields after impact. Additionally, a digital twin model has been successfully developed for pipe-shaped specimens. The findings discussed above provide valuable insights that contribute to enhancing performance and preventing failures during the design and manufacturing phases of CIPP liner systems.